REVISION 1

An X-ray diffraction study of the pressure-induced hydration in cordierite at 4-5 GPa

Anna Yu. Likhacheva,* Sergey V. Goryainov, and Taras A. Bul'bak

Sobolev Institute of Geology and Mineralogy SibD RAS, Novosibirsk, Russia

Abstract

The elastic and structure behavior of natural cordierite compressed in aqueous medium up to 6 GPa was studied by means of in situ synchrotron powder diffraction with a diamond anvil cell. In the range between 1-4 GPa the elastic behavior is regular and slightly anisotropic, with linear compressibilities β_a:β_b:β_c=4:4:5, the most rigid *a*-*b* plane coinciding with the orientation of 6-membered rings. A distinct decrease of compressibility in the range of 4-5 GPa indicates a pressure-induced hydration (PIH), which is confirmed by the structure refinements. The addition of about 60% of the initial water content into the cordierite channels proceeds through positional disordering of the H_2O sites inside the channel cavity and a stepwise filling of the H_2O position inside the 6-membered rings, leading to the phase transition at about 4.7 GPa. The appearance of H_2O molecules inside 6-membered rings prevents their contraction and even causes their slight enlargement along *a* direction, apparently related to the orientation of H-bonds. This results in anisotropic deformation of the unit cell and the increase of *a* parameter in the H*P* phase at 4.9 GPa, as well as the decrease of linear compressibility along *a* upon the further compression up to 6 GPa (β_a:β_b:β_c=5:9:10).

Key-words: cordierite, high pressure, compressibility, pressure-induced hydration, crystal structure.

Introduction

Cordierite, a ring framework aluminosilicate $(Mg,Fe)_2[Al_4Si_5O_{18}]*n(H_2O,CO_2)$, has attracted much interest due to its widespread formation in moderate- to high-grade metamorphic

rocks, as well as due to its channel structure accessible for small molecules (predominantly H_2O and CO_2) (Shreyer and Yoder 1964; Gibbs 1966; Cohen et al. 1977; Goldman et al. 1977; Hochella 1979; Armbruster 1985; Poon et al. 1990; Le Breton and Schreyer 1993; Lepezin et al. 1999; Toohill et al. 1999; Kolesov and Geiger 2000; Bul'bak and Shvedenkov 2005). Despite its petrological importance, only few works were devoted to the high-pressure behavior of cordierite (Mirwald 1982; Mirwald et al. 1984; Koepke and Schulz 1986). In the low pressure region the volume compressibility of cordierite (K_0=90 GPa) is close to that of feldspars, whereas in the range of 1-3 GPa it approaches the order of that of beryl (K_0=143 GPa) (Mirwald et al. 1984; Hazen et al. 1986). This indicates a dominant role of the ring elements in compression behavior of cordierite structure. In the cordierite structure, the 6-membered $(Si,Al)O_4$-tetrahedral rings (6mR) form channels by stacking along the *c*-direction. The rings are included in a frame of edge-sharing $(Mg,Fe)O_6$ octahedra and $(Si,Al)O_4$-tetrahedra, with the octahedra located between the ring planes (Gibbs 1966; Cohen et al. 1977).

The compression behavior of "empty" (waterless) cordierite was found to depend on the type of pressure-transmitting medium. In a non-penetrating (methanol-ethanol) medium, the compression is approximately regular up to 3 GPa, whereas in penetrating water medium it sharply decreases at P>2 GPa due to the incorporation of excess H_2O molecules (Koepke and Schulz 1986). At that, a significant shrinking of 6mR tetrahedra was observed, which was supposed to introduce a phase transition at higher pressure. Indeed, our recent Raman spectroscopic study has revealed a reversible, low-kinetics phase transition in natural cordierite upon the compression in aqueous medium up to about 4.7 GPa (Likhacheva et al. 2012). This transition is evinced by the abrupt shifts of all the framework and O-H stretching modes. The shift magnitudes of different framework modes indicate the predominance of distortion over contraction of the framework polyhedra upon this transition. However, the influence of penetrating water medium onto the observed transition remains unclear. Since there is no structural data on the H*P*-behavior of cordierite at P>2.5 GPa, the present study aims at a

detailed description of the elastic and structural behavior of cordierite in the pressure interval between 2 and 6 GPa, and, in particular, the elucidation of the penetrating role of water in the observed phase transition.

Experimental

A sample of cordierite (Z-cordierite) used in this study is from the Altai amphibolite complex (Russia), with the chemical formula $Na_{0.07}(Mg_{1.57}Fe_{0.36}Mn_{0.07})[Al_{3.96}Fe_{0.06}Si_{4.98}O_{18}]$ $*0.45H_2O$ (the average from 7 microprobe analyses). The same sample was used in the H*P* Raman study of Likhacheva et al. (2012). It presents homogenous, inclusion-free, transparent and uniformly colored grains. The H_2O content was determined by gas chromatographic analysis with the accuracy of 0.08 wt%. The cell parameters at ambient conditions determined by Rietveld refinement are a = 17.104(2), b = 9.746(1), c = 9.333(1) Å, V = 1555.7(2) $Å^3$, space group *Cccm*. The powdered sample was placed into a 400×100 μm gasket hole of a diamond anvil cell (DAC) and compressed up to 6 GPa. The DAC is based on a modified Mao-Bell design (Fursenko et al. 1984) and employs two diamonds with 1 mm diameter culets. Two H*P* experiments were carried out using both penetrating (H_2O+30% methanol:ethanol 4:1) and non-penetrating (methanol:ethanol 4:1) medium. The pressure values were measured before and after the diffraction experiment from the R1 ruby fluorescence line (Mao et al. 1986) excited by a 514 nm line of Ar laser. The powder diffraction experiments were performed at the 4^{th} beamline of the VEPP-3 storage ring of Synchrotron center SSTRC of the Institute of nuclear physics, Novosibirsk (Ancharov et al. 2001), at a constant wavelength of 0.3685 Å. An MAR345 imaging plate detector (pixel dimension 100 μm) was used. The sample to detector distance was 368 mm, and the focused X-ray beam was 100×100 $μm^2$ in size. The program FIT2D (Hammersley et al. 1996) was used for integrating the two-dimensional images up to $2\Theta_{max} = 25^o$. The lattice parameters of cordierite at different pressures were refined by whole pattern fitting using the Rietveld method, with the GSAS package (Larson and Von Dreele 2000). The diffraction

profiles collected at ambient pressure (hereafter 0 GPa), 4.4 and 4.9 GPa (in aqueous medium) were used for the structure refinements.

Rietveld refinement of the crystal structure was performed using data in the 2θ range 3-25°. The instrumental background was approximated by a Chebyshev polynomial with 28 coefficients. The Bragg peak profiles were refined by a pseudo-Voight function. The scattering factors for silicon, aluminum and sodium atoms were used to model the framework (Si,Al) and extra-framework species (Na), respectively. To model the H_2O molecules, we used the scattering factor for fluorine atom, providing a better approximation to the scattering capability of H_2O molecule in comparison with oxygen atom, as it was shown earlier (Seryotkin et al. 2003). The Si-O and Al-O distances were restrained to 1.61(2) Å and 1.75(2) Å, respectively; the restraints were removed only in several final cycles of the refinement. The U_{iso} values assigned to (Mg,Si,Al), O, Na and F atoms were taken from the data of Sokol et al. (2010) and Koepke and Shulz (1986). Due to a narrow 2θ range used, the U_{iso} values for all atoms were not refined. The crystal structure of natural (Mg,Fe)-cordierite (Hochella et al. 1979) was used as a starting model for the refinement of the L*P* structure at 0 GPa. The H*P* structures were derived from the refined L*P* structure with addition of a new H_2O split site close to the original position Ow1 in the channel, as well a new H_2O site inside 6mR. The final refined structure parameters were the atomic coordinates (for all the atoms) and the occupancy factors for the H_2O sites.

Results and discussion

Variation of the lattice parameters at high water pressure

During the compression in aqueous medium up to 6 GPa, no change in the profile shape of Z-cordierite is observed, which indicates the preservation of the original space group *Cccm* at high pressure. In the pressure range between 0-4 GPa the compression is slightly anisotropic (Fig. 1a), in agreement with Brillouin measurements of Toohill et al. (1999). The mean axial compressibilities estimated from linear regressions ($\beta_a = \beta_b = 2.4(1)\cdot10^{-3}$, $\beta_c = 3.1(1)\cdot10^{-3}$ GPa^{-1}) are similar to the previous data of Mirwald et al. (1984) and Koepke and Schulz (1986) obtained

for non-penetrating medium. The less compressible plane *a*-*b* is parallel to the orientation of rigid 6mR. Within the pressure range of 0-4 GPa, the two sets of the volume data obtained using both penetrating and non-penetrating medium closely coincide (Fig. 1b). Therefore, the *P*-*V* data for the compression in aqueous medium at 0-4 GPa and those obtained for the compression in non-penetrating medium at 0-5.5 GPa were used as a whole to estimate the elastic parameters. Fitting the volume data with Murnaghan EoS (Murnaghan 1937, Angel 2001) gives: V_0 = 1569(2) Å^3, K_0 = 115(3) GPa, K' = 4 (fixed) (Fig. 1a). The K_0 value is slightly lower than K_0 = 129(1) GPa obtained from Brillouin measurements by Toohill et al. (1999), and is intermediate between the K_0 values of 91(5) and 143(5) GPa found by Mirwald et al. (1984) for the pressure ranges of 0-1 and 1-3 GPa.

In the pressure range between 4 and 4.4 GPa, the volume compressibility of Z-cordierite in aqueous medium is lowered to almost zero (Fig. 1b, Table 1) due to a substantial drop of the compressibility along *a* and *b* directions. This may be regarded as an indirect evidence for a pressure-induced hydration (PIH) of the framework channels. A similar decrease of compressibility due to PIH was observed by Koepke and Schulz (1986) in "empty" cordierite at 2.3 GPa. The comparison with the volume data obtained in non-penetrating medium at $P > 3.5$ GPa (Fig. 1b) argues for the observed compression anomaly to be due to the penetrating function of water.

Upon the pressure rise up to 4.9 GPa, an anisotropic volume expansion of ≈ 0.1 % results from the predominant increase of the *a* parameter and less enlargement along *c*, whereas the *b* parameter does not change. Upon the further compression at $P > 5$ GPa the *a* and *b* compressibilities change into opposite directions, whereas the compressibility along *c* and the bulk modulus retain the initial value: $\beta_a = 1.6(1)\cdot10^{-3}$, $\beta_b = 2.7(1)\cdot10^{-3}$, $\beta_c = 3.0(1)\cdot10^{-3}$ GPa^{-1}, K_0 = 115(2) GPa (fitting with Murnaghan EoS, K' = 4 (fixed)). This change of the compression mechanism is apparently related with the transition to a new H*P* phase associated with PIH in the pressure range between 4.4 and 4.9 GPa. The existence of phase transition is in line with the

previous spectroscopic data showing the abrupt shifts of the Raman bands in Z-cordierite in the same pressure interval (Likhacheva et al. 2012).

Based on the observed deviation from regular compression at $P > 4$ GPa, we can suppose that the transition to the H*P* phase is preceded by the formation of intermediate PIH state of cordierite structure in the pressure range between 4 and 4.5 GPa.

The crystal structure of Z-cordierite at 4.4 and 4.9 GPa

Refinement details for the L*P* and H*P* structures of Z-cordierite are reported in Table 2, and the refined atomic parameters at 0, 4.4 and 4.9 GPa are given in Tables 3 and 4. The Rietveld plots and the L*P* and H*P* structures are drawn in Figures 2 and 3, correspondingly. In the L*P* structure at 0 GPa all the distances and angles in the framework polyhedra are in reasonable agreement with the previous single-crystal data (Hochella et al. 1979; Yakubovich et al. 2004). The refined occupancy of Na site in the center of 6mR and that of H_2O (Ow1) site located in the large cavity of the channel (Fig. 3a, Table 3) agree with the data of chemical analysis.

Based on the compression trends described above, we consider the H*P* structures refined at 4.9 and 4.4 GPa to represent the H*P* phase and its precursor, correspondingly. As compared to the L*P* structure, the occupancy of the position at 0,0,0 in the center of 6mR gradually increases in the precursor and H*P* phase (Table 3). We should emphasize that the increase of the 0,0,0 occupancy in both structures was obtained in several repeated refinements. Provided the Na occupancy was fixed at the initial value of 0.08, the observed increase of the 0,0,0 occupancy is obviously related with the penetration of extra H_2O molecules from the pressure-transmitting medium. The H_2O position inside the 6mR was labeled as Ow3 (Figs. 3b,c, Tables 3,4). Due to the appearance of H_2O inside 6mR, we had to introduce into the structure model an additional H_2O site (Ow2) slightly shifted from the initial position Ow1 in the center of channel cavity (Figs. 3b,c), in order to provide a reasonable distance to the site Ow3 inside 6mR (Table 4). This has led to redistribution of the occupancy factors between the Ow1 and Ow2 sites inside the

156 channel cavity (Table 3), the total (Ow1+Ow2) occupancy being increased by about 20% of the
157 initial value in the precursor phase at 4.4 GPa (Table 3). Appreciable lowering of R-factor
158 confirmed the addition of the position Ow2 to be reasonable. It should also be noted that the
159 positional disordering of H_2O inside the cage due to the appearance of Ow2 agrees with the
160 observed broadening of the intense Raman band of O-H stretching vibrations (Likhacheva et al.
161 2012).

162 Taking into account the contribution of new H_2O sites Ow2 and Ow3, the total amount of
163 water in Z-cordierite increases from 0.45 (0 GPa) to 0.69 and 0.72 molecules (per 18 oxygens) in
164 the precursor and H*P* phase, correspondingly (Table 2). At that, the increase of the water content
165 in the H*P* phase proceeds only at the expense of additional filling of the Ow3 site inside 6mR
166 (Table 3), which can therefore be regarded as a driving force for this transition.

167 The appearance of H_2O molecules inside 6mR prevents the contraction of these rings
168 along *a* direction, which is seen from the preservation of the initial O2-O2 distance in 6mR in
169 both the H*P* structures (Fig. 3a, Table 4). It seems reasonable to suppose the H-vectors of H_2O
170 molecule inside 6mR to be oriented towards O2 atoms, because the Ow3-O2 distance of ≈ 2.98
171 Å (Table 4) is the only favorable for the accommodation of H-bond. This supposition is in line
172 with the observed anisotropic deformation of the unit cell and the increase of *a* parameter upon
173 the transition at ≈ 4.7 GPa, as well as the decrease of linear compressibility along *a* during the
174 further compression up to 6 GPa.

175 The (Mg,Fe)-O_6 octahedra, presenting the "inner" part of the cordierite framework,
176 contract almost uniformly. The Si(2)O_4- and AlO_4-tetrahedra, joining octahedral polyhedra and
177 6mR, undergo an anisotropic deformation without contraction: the mean (Si,Al)-O distances in
178 these tetrahedra remain at the initial level in both the H*P* structures. The Si(2)O_4-tetrahedron
179 expands along *a* and slightly contracts along the *c* direction, whereas the AlO_4-tetrahedron
180 contracts mainly along the *c* axis. On the whole, both the precursor and H*P* phases are
181 characterized by similar PIH level and associated deformation of the framework. The structure of

the H*P* phase at 4.9 GPa differs from its precursor by a minor increase of H_2O content and slight concerted rotation and twisting of all the framework polyhedra. This smooth transition is apparently driven by exceeding some critical amount of extra H_2O entering the Ow3 site inside 6mR, as it is mentioned above.

The location of H_2O molecules in a "tight" position inside the 6mR, commonly occupied only by cations in natural cordierites (Cohen et al. 1977; Armbruster 1985; Yakubovich et al. 2004), is quite unusual. Another example of such an "exotic" siting is provided by the high-temperature structural study of natural H_2O-bearing cordierite (Hochella et al. 1979). It is noteworthy that a minor amount of H_2O inside the 6mR was located only in the sample cooled down to room temperature after partial dehydration at 775°C. Therefore, the H_2O molecules appeared inside the 6mR as a result of their re-distribution throughout the framework channel "quenched" by a relatively quick cooling. It seems probable that in both the H*P* and H*T* experiments the appearance of H_2O inside the 6mR reflects a kinetically hindered character of water diffusion in cordierite channels, which is known to stop in the temperature range between 200° and 300°C (Bul'bak et al. 2005). It is interesting that the compression in aqueous medium not only provides the formation of such a "non-equilibrium" distribution of H_2O molecules throughout the cordierite channel, but even makes the new H*P* phase quasi-stable in a certain pressure range, according to a regular compression at $P > 5$ GPa.

To summarize, the presented structural data reveal the formation of PIH state and associated phase transition in natural H_2O-bearing cordierite in the pressure range between 4.4 and 5 GPa. This is about 2.5 GPa higher than the pressure needed for PIH in "empty" cordierite (Koepke and Schulz 1986). The enlargement and lowering of the lattice compressibility along *a* axis is related to the penetration of H_2O molecules preventing the contraction of the channel-forming 6mR. This is an unusual case when a nearly isotropic compressibility of cordierite within the *a*-*b* plane is violated under the influence of H_2O molecules residing in 6mR. This H*P* behavior differs from the deformation mechanism observed at high temperature, where the

208 expansion along *a* and *b* axes proceeds at the expense of the enlarged Mg-octahedra, the 6mR
209 remaining undeformed (Hochella et al. 1979).

210 **Acknowledgements.** The authors are grateful to Dr. Yu.V. Seryotkin for helpful discussion of
211 the material, and we thank Prof. G.G. Lepezin for providing the cordierite sample. This work is
212 supported by the Ministry of Education and Science of the Russian Federation. The work was
213 carried out involving the equipment belonging to the SSTRC. The support of RAS program
214 ONZ-9 and RFBR grant # 11-05-01121 is acknowledged.

215 **References**

216 Ancharov, A.I., Manakov, A.Yu., Mezentsev, N.A., Tolochko, B.P., Sheromov, M.A., and
217 Tsukanov V.M. (2001) New station at the 4th beamline of the VEPP-3 storage ring. Nuclear
218 Instruments and Methods of Physical Research A, 470, 80-83.

219 Angel, R.I. (2001) EOS-FIT V6.0 Computer program. Crystallography Laboratory, Department
220 of Geological Sciences, Virginia Tech, Blacksburg, U.S.A.

221 Armbruster, Th. (1985) Ar, N_2 and CO_2 in the structural cavities of cordierite, an optical and x-
222 ray single-crystal study. Physics and Chemistry of Minerals, 12, 233-245.

223 Bul'bak, T.A. and Shvedenkov, G.Yu. (2005) Experimental study of incorporation of C-H-O-N
224 fluid components in Mg-cordierite. European Journal of Mineralogy, 17, 829-838.

225 Bul'bak, T.A., Shvedenkov, G.Yu., and Ripinen, O.I. (2005) Kinetics of H_2O-CO_2 molecular
226 exchange in the structural channels of (Mg,Fe^{2+})-cordierite. Geochemistry International, 43,
227 386-394.

228 Cohen, J.P., Ross, F.K., and Gibbs, G.V. (1977) An x-ray and neutron diffraction study of
229 hydrous low cordierite. American Mineralogist, 62, 67-75.

230 Fursenko, B.A., Litvin, Yu.A., and Kropachev, V.D. (1984) Apparatus with transparent anvils-
231 windows for optical and X-ray studies at high pressures. Pribory I Technika Experimenta,
232 174-178 (in Russian).

Gibbs, G.V. (1966) The polymorphism of cordierite I: the crystal structure of low cordierite. American Mineralogist, 51, 1068-1087.

Goldman, D.S., Rossman, G.R., and Dollase, W.A. (1977) Channel constituents in cordierite. American Mineralogist, 62, 1144-1157.

Hammersley, A.P., Svensson, S.O., Hanfland, M., Fitch, A.N., and Hausermann, D. (1996) Two-dimensional detector software: from real detector to idealized image or two-theta scan. High-Pressure Research, 14, 235-248.

Hazen, R.M., Au, A.Y., and Finger, L.W. (1986) High-pressure crystal chemistry of beryl ($Be_3Al_2Si_6O_{18}$) and euclase ($BeAlSiO_4OH$). American Mineralogist, 71, 977-984.

Hochella, M.F., Brown, G.E., Ross, F.K., and Gibbs, G.V. (1979) High-temperature crystal chemistry of hydrous Mg- and Fe-cordierites. American Mineralogist, 64, 337-351.

Koepke, J. and Schulz, H. (1986) Single crystal structure investigations under high-pressure of the mineral cordierite with an improved high-pressure cell. Physics and Chemistry of Minerals, 13, 165-173.

Kolesov, B.A. and Geiger, C.A. (2000) Cordierite II: The role of CO_2 and H_2O. American Mineralogist, 85, 1265-1274.

Kolesov, B.A. (2006) Raman spectra of single H_2O molecules isolated in the crystal cavities. Journal of Structure Chemistry, 47, 27-40.

Larson, A.C. and Von Dreele, R.B. (2000) General structure analysis system (GSAS). Report LAUR 86-748, Los Alamos National Lab, New Mexico 2000.

Le Breton, N. and Schreyer, W. (1993) Experimental CO_2 incorporation into Mg-cordierite: nonlinear behavior of the system. European Journal of Mineralogy, 5, 427-438.

Lepezin, G.G., Bul'bak, T.A., Sokol, E.V., and Shvedenkov, G.Yu. (1999) Fluid components in cordierites and their significance for metamorphic petrology. Russian Geology and Geophysics, 40, 99-116.

Likhacheva, A.Yu., Goryainov, S.V., Krylov, A.S., Bul'bak, T.A., and Prasad, P.S.R. (2012) Raman spectroscopy of natural cordierite at high water pressure up to 5 GPa. Journal of Raman spectroscopy, 43, 559-563.

Mao, H.K., Xu, J., and Bell, P.M. (1986) Calibration of the ruby pressure gauge to 800 kbar under quasi-hydrostatic conditions. Journal of Geophysical Research, 91, 4673-4676.

Mirwald, P.W. (1982) A high-pressure phase transition in cordierite. American Mineralogist, 67, 277-283.

Mirwald, P.W., Malinowski, M., and Schulz, H. (1984) Isothermal compression of low-cordierite to 30 kbar. Physics and Chemistry of Minerals, 11, 140-148.

Murnaghan, F.D. (1937) Finite deformations of an elastic solid. American Journal of Mathematics, 49, 235-260.

Poon, W.C.K., Putnis, A., and Salje, E. (1990) Structural states of Mg cordierite: IV. Raman spectroscopy and local order parameter behavior. Journal of Physics: Condensed Matter, 2, 6361-6372.

Seryotkin, Yu.V., Joswig, W., Bakakin, V.V., Belitsky, I.A., and Fursenko, B.A. (2003) High-temperature crystal structure of wairakite. European Journal of Mineralogy, 15, 475-484.

Shreyer, W. and Yoder, H.S. (1964) The system Mg-cordierite – H_2O and related rocks. Neues Jahrbuch fur Mineralogie Abhandlungen, 101, 271-34.

Sokol, E.V., Seryotkin, Yu.V., and Bul'bak, T.A. (2010) Na-Li-Be-rich cordierite from the Murzinka pegmatite field, Middle Urals, Russia. European Journal of Mineralogy, 22, 565-575.

Toohill, K., Siegesmund, S., and Bass, J.D. (1999) Sound velocities and elasticity of cordierite and implications for deep crustal seismic anisotropy. Physics and Chemistry of Minerals, 26, 333-343.

Yakubovich, O.V., Massa, W., Pekov, I.V., Gavrilenko, P.G., and Chukanov, N.V. (2004) Crystal structure of the Na,Ca,Be-cordierite and crystal chemical regularities in the cordierite-sekaninaite series. Crystallography Reports, 49, 953-963.

Captions for figures

Fig.1. Pressure dependence of the normalized lattice parameters (a) and volume (b) of Z-cordierite compressed in aqueous medium. The volume curve obtained using an aqueous medium (filled squares) is compared with our data (empty squares) and the data of Mirwald et al. (1984) (dotted line) for the compression in non-penetrating alcohol medium in DAC. The Murnaghan EoS fit is shown by solid line.

Fig.2. Rietveld refinements of Z-cordierite at 0 GPa (a) and 4.9 GPa (b). The observed and calculated profiles are indicated by (+) and by a continuous line, respectively. The tick marks indicate the positions of allowed Bragg peaks in the respective symmetry. A difference curve is plotted at the bottom. The demonstrated diffraction profile is limited to the region of $2\theta=2.5\text{-}14^{o}$ because this part is the most representative: it contains all the intense reflections of Z-cordierite and is free from the peaks of ice 7.

Fig.3. Crystal structure of Z-cordierite at 0 GPa (a), 4.4 GPa (b) and 4.9 GPa (c).

Table 1. Lattice parameters of Z-cordierite (space group *Cccm*) at compression up to 6 GPa.

***P* (GPa)**	***a* (Å)**	***b* (Å)**	***c* (Å)**	***V* (Å^3)**
Compression in aqueous medium (H_2O+30% methanol:ethanol 4:1)				
0	17.104(2)	9.746(1)	9.333(1)	1555.7(2)
1.4	17.047(3)	9.711(2)	9.293(2)	1538.4(3)
2.0	17.021(2)	9.692(1)	9.274(1)	1529.9(2)
2.6	16.987(3)	9.683(1)	9.252(1)	1521.8(3)
3.0	16.976(3)	9.670(2)	9.246(1)	1517.7(3)
3.5	16.969(4)	9.660(2)	9.231(2)	1513.2(5)
3.85	16.944(3)	9.659(1)	9.221(1)	1509.2(3)
4.4	16.944(2)	9.656(1)	9.216(1)	1507.8(2)
4.9	16.959(1)	9.653(1)	9.217(1)	1508.9(2)
5.6	16.941(3)	9.633(1)	9.200(1)	1501.3(3)
6.15	16.924(3)	9.621(1)	9.182(1)	1495.0(3)
Compression in methanol:ethanol 4:1				
1.3	17.051(4)	9.703(2)	9.307(2)	1539.8(4)
2.05	17.017(4)	9.692(3)	9.280(2)	1530.5(4)
3.5	16.966(1)	9.639(7)	9.230(6)	1510(2)
4.5	16.914(7)	9.625(4)	9.203(4)	1498(1)
5.2	16.867(8)	9.625(5)	9.200(4)	1494(1)

Table 2. Basic crystallographic and experimental data for Z-cordierite at high pressures.

Pressure (GPa)	0	4.4	4.9
a (Å)	17.104(2)	16.944(2)	16.959(1)
b (Å)	9.746(1)	9.656(1)	9.653(1)
c (Å)	9.333(1)	9.216(1)	9.217(1)
V (Å^3)	1555.7(2)	1507.8(2)	1508.9(2)
Space group	*Cccm*		
Radiation	λ = 0.3685 Å		
2Θ range (^{o})	3-25		
Number of observations	2443		
Number of variables	60	65	68
Number of reflections	650	650	650
R_p	0.004	0.004	0.006
R_{wR}	0.005	0.005	0.009
R_F^2	0.10	0.15*	0.13*
χ^2	0.23	0.21	0.34
Calculated amount of H_2O mol./f.u. (18 oxygens)	0.45(1)	0.69(2)	0.72(1)

* The R_F^2 values are higher than that for 0 GPa because several regions are excluded from the refinement due to the presence of ice 7

Table 3. Atomic coordinates for Z-cordierite at 0, 4.4 and 4.9 GPa.

Atom	*P, GPa*	*x/a*	*y/b*	*z/c*	*Occupancy*	U_{iso}
Mg	0	0.163(1)	0.5000000(0)	0.2500000(0)	1.000(0)	0.008
	4.4	0.1625(2)	0.5000000(0)	0.2500000(0)	1.000(0)	0.008
	4.9	0.164(1)	0.5000000(0)	0.2500000(0)	1.000(0)	0.008
Si(1)	0	0.193(1)	0.079(1)	0.0000000(0)	1.000(0)	0.008
	4.4	0.1933(2)	0.0796(3)	0.0000000(0)	1.000(0)	0.008
	4.9	0.192(1)	0.082(1)	0.0000000(0)	1.000(0)	0.008
Si(2)	0	0.0000000(0)	0.5000000(0)	0.2500000(0)	1.000(0)	0.008
	4.4	0.0000000(0)	0.5000000(0)	0.2500000(0)	1.000(0)	0.008
	4.9	0.0000000(0)	0.5000000(0)	0.2500000(0)	1.000(0)	0.008
Si(3)	0	-0.137(1)	0.236(1)	0.0000000(0)	1.000(0)	0.008
	4.4	-0.1378(2)	0.2372(3)	0.0000000(0)	1.000(0)	0.008
	4.9	-0.139(1)	0.233(1)	0.0000000(0)	1.000(0)	0.008
Si(4)	0	0.049(1)	0.309(1)	0.0000000(0)	1.000(0)	0.008
	4.4	0.050(1)	0.313(1)	0.0000000(0)	1.000(0)	0.008
	4.9	0.050(1)	0.318(1)	0.0000000(0)	1.000(0)	0.008
Al	0	0.2500000(0)	0.2500000(0)	0.251(3)	1.000(0)	0.008
	4.4	0.2500000(0)	0.2500000(0)	0.248(1)	1.000(0)	0.008
	4.9	0.2500000(0)	0.2500000(0)	0.258(2)	1.000(0)	0.008
O(1)	0	0.247(1)	0.102(2)	0.144(2)	1.000(0)	0.01
	4.4	0.2468(2)	0.0984(4)	0.1435(3)	1.000(0)	0.01
	4.9	0.247(1)	0.103(2)	0.146(1)	1.000(0)	0.01
O(2)	0	-0.168(1)	0.081(3)	0.0000000(0)	1.000(0)	0.01
	4.4	-0.171(1)	0.0831(3)	0.0000000(0)	1.000(0)	0.01
	4.9	-0.170(1)	0.079(2)	0.0000000(0)	1.000(0)	0.01
O(3)	0	0.123(1)	0.187(2)	0.0000000(0)	1.000(0)	0.01
	4.4	0.1232(3)	0.190(1)	0.0000000(0)	1.000(0)	0.01
	4.9	0.122(1)	0.191(2)	0.0000000(0)	1.000(0)	0.01
O(4)	0	0.064(1)	0.416(1)	0.154(1)	1.000(0)	0.01
	4.4	0.0647(3)	0.413(1)	0.153(1)	1.000(0)	0.01
	4.9	0.066(1)	0.410(1)	0.159(1)	1.000(0)	0.01
O(5)	0	-0.044(1)	0.249(2)	0.0000000(0)	1.000(0)	0.01
	4.4	-0.0436(2)	0.247(2)	0.0000000(0)	1.000(0)	0.01
	4.9	-0.044(1)	0.249(2)	0.0000000(0)	1.000(0)	0.01
O(6)	0	-0.172(1)	0.313(1)	0.143(1)	1.000(0)	0.01
	4.4	-0.1706(3)	0.3152(3)	0.1424(3)	1.000(0)	0.01
	4.9	-0.172(1)	0.317(1)	0.140(1)	1.000(0)	0.01
Na	0	0.0000000(0)	0.0000000(0)	0.0000000(0)	0.08(1)	0.025
	4.4	0.0000000(0)	0.0000000(0)	0.0000000(0)	0.08	0.025
	4.9	0.0000000(0)	0.0000000(0)	0.0000000(0)	0.08	0.025
Ow1	0	0.0000000(0)	0.0000000(0)	0.2500000(0)	0.45(1)	0.1
	4.4	0.0000000(0)	0.0000000(0)	0.2500000(0)	0.13(2)	0.1
	4.9	0.0000000(0)	0.0000000(0)	0.2500000(0)	0.12(1)	0.1
Ow2	4.4	0.01(2)	0.02(3)	0.32(1)	0.110(5)	0.1
	4.9	-0.01(2)	-0.03(2)	0.318(5)	0.115(4)	0.1
Ow3	4.4	0.0000000(0)	0.0000000(0)	0.0000000(0)	0.12(2)	0.1
	4.9	0.0000000(0)	0.0000000(0)	0.0000000(0)	0.14(1)	0.1

Table 4. Selected structural parameters for Z-cordierite at compression in aqueous medium.

		0 GPa	4.4 GPa	4.9 GPa
6-ring				
O(2) – O(2)	∥a	5.96(3)	5.99(1)	5.95(2)
O(3) – O(3)	∥a	5.56(3)	5.56(1)	5.53(2)
O(5) – O(5)	∥b	5.07(3)	4.99(1)	5.03(2)
mean diameter		**5.53**	**5.51**	**5.50**
Si(1) – O(1)	x2	1.65(1)	1.614(2)	1.65(1)
O(2)		1.61(3)	1.617(3)	1.60(2)
O(3)		1.59(2)	1.598(3)	1.60(2)
mean		**1.63**	**1.61**	**1.62**
Si(3) – O(2)		1.60(3)	1.588(3)	1.58(2)
O(5)		1.60(3)	1.599(3)	1.63(2)
O(6)	x2	1.64(1)	1.605(2)	1.62(1)
mean		**1.62**	**1.60**	**1.61**
Si(4) – O(3)		1.73(2)	1.71(1)	1.72(2)
O(4)	x2	1.79(1)	1.73(1)	1.74(1)
O(5)		1.70(3)	1.71(2)	1.72(2)
mean		**1.75**	**1.72**	**1.73**
(Mg,Fe) – O(1)	x2	2.08(2)	2.056(3)	2.05(2)
O(4)	x2	2.10(2)	2.060(4)	2.06(2)
O(6)	x2	2.08(2)	2.060(2)	2.04(1)
mean		**2.08**	**2.06**	**2.05**
O(1) – O(1)	∥b	5.07(2)	4.98(1)	5.01(2)
Al – O(1)	x2	1.76(2)	1.751(3)	1.76(2)
O(6)	x2	1.77(2)	1.792(3)	1.75(2)
mean		**1.765**	**1.77**	**1.755**
O(1) – O(6)	∥c	4.92(3)	4.89(1)	4.82(2)
O(1) – O(1)	∥b	2.89(3)	2.93(1)	2.84(2)
Si(2) – O(4)		**1.63(1)**	**1.64(1)**	**1.65(1)**
O(4) – O(4)	∥c	2.43(2)	2.44(1)	2.41(2)
O(4) – O(4)	∥a	3.95(2)	3.94(1)	4.07(2)
Na/Ow3 – O(2)	x2	2.98(2)	3.00(1)	2.98(2)
– O(3)	x2	2.78(2)	2.78(1)	2.77(2)
– O(5)	x2	2.54(2)	2.50(2)	2.52(1)
– Ow1		2.3333(2)	2.3040(2)	2.3043(2)
– Ow2			2.9(1)	2.95(5)

Fig.1a

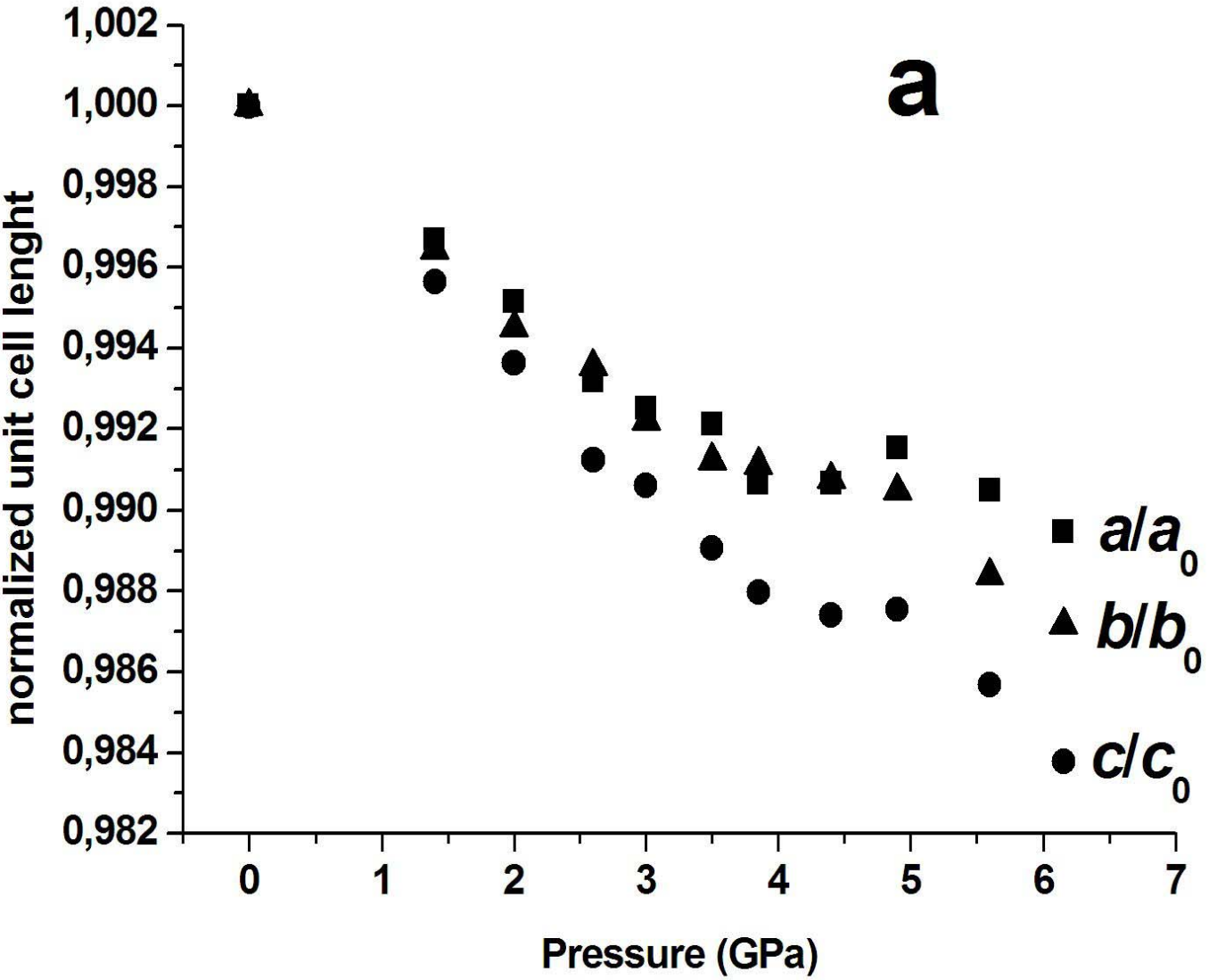
a
normalized unit cell lenght
1,002
1,000
0,998
0,996
0,994
0,992
0,990
0,988
0,986
0,984
0,982
0
1
2
3
4
5
6
7
Pressure (GPa)
a/a0
b/b0
c/c0

Fig.1b

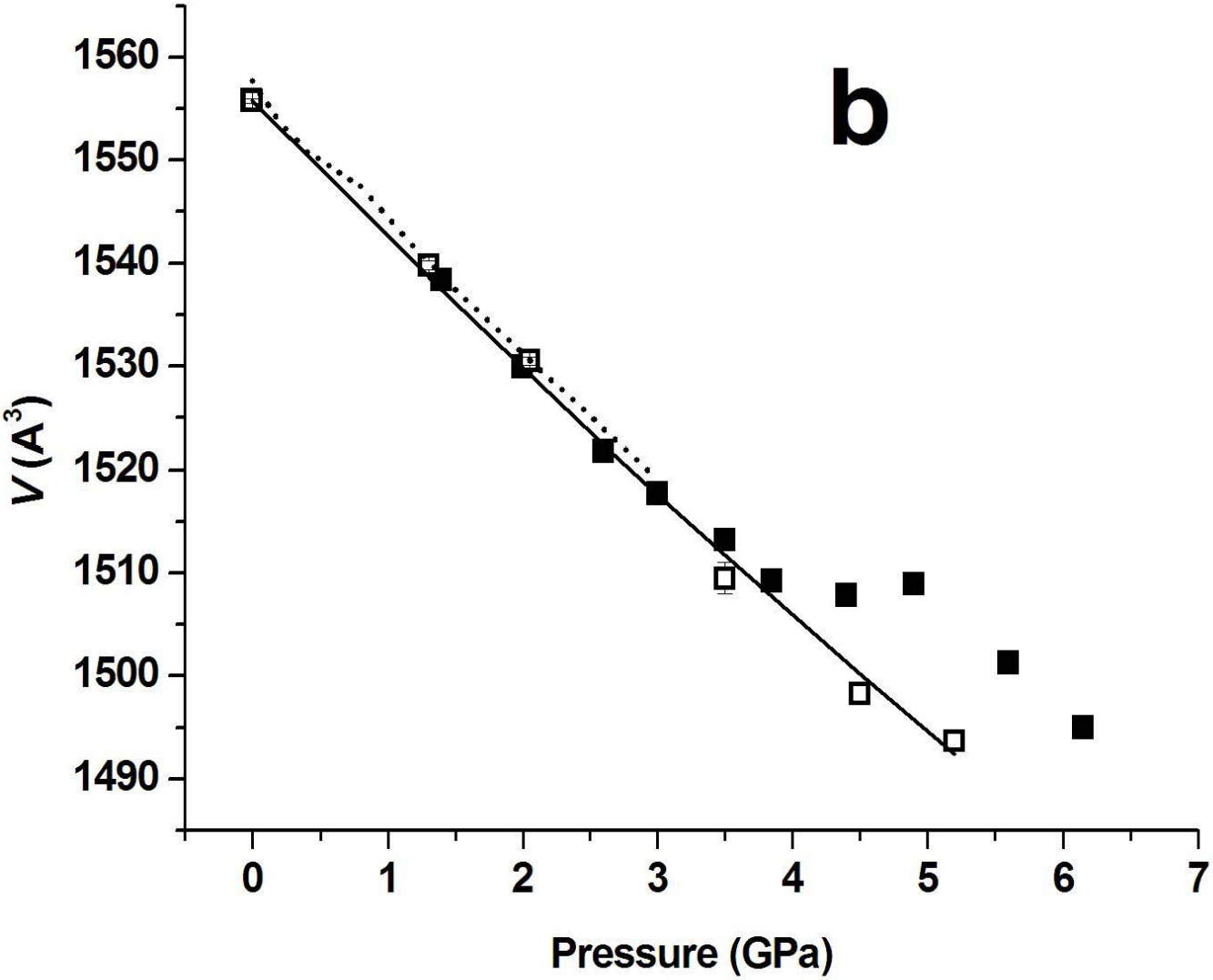
b
1560
1550
1540
1530
1520
1510
1500
1490
V (A3)
0
1
2
3
4
5
6
7
Pressure (GPa)

Fig.2a

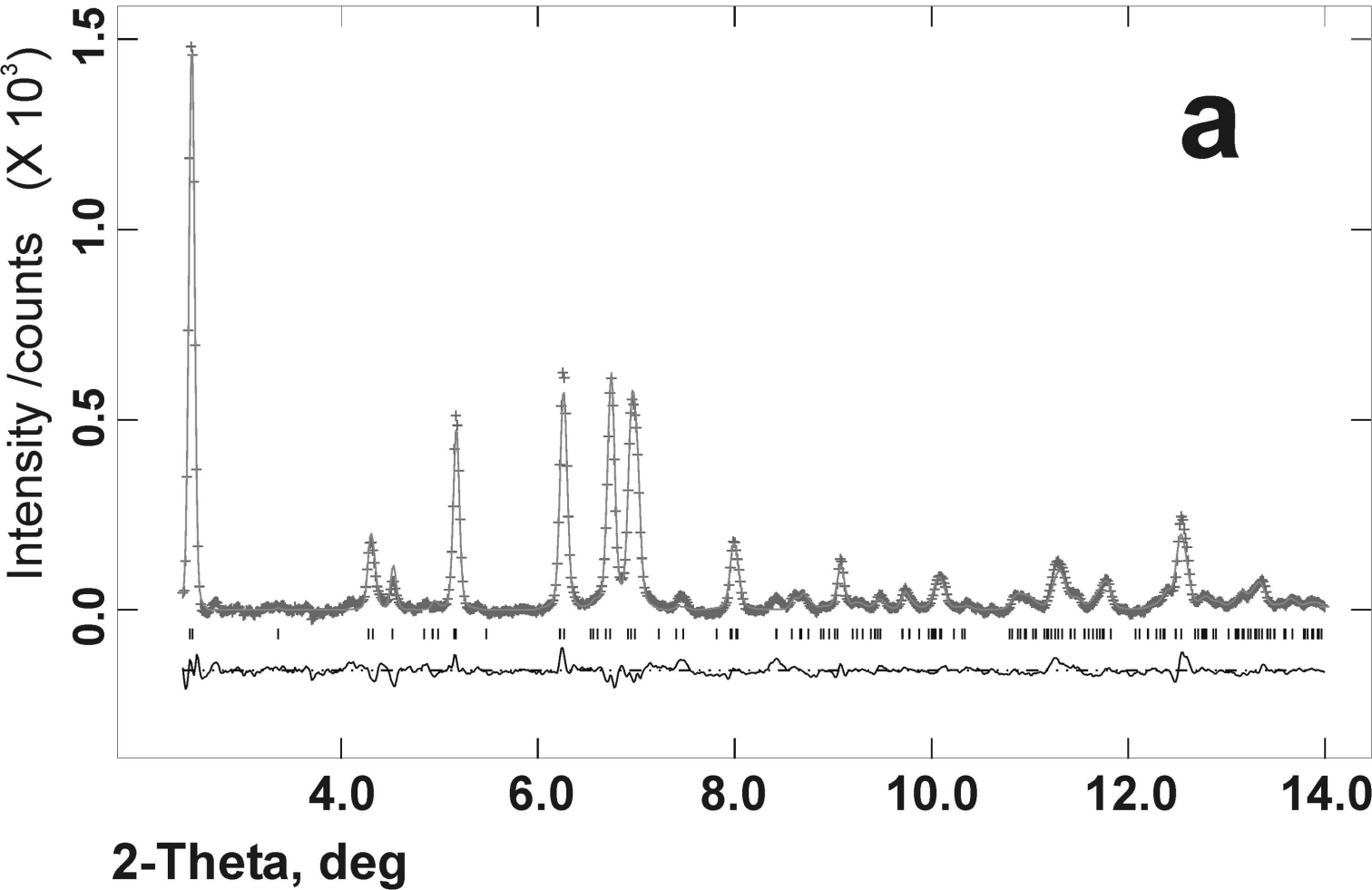
a
Intensity /counts (X 10^3)
0.0
0.5
1.0
1.5
4.0
6.0
8.0
10.0
12.0
14.0
2-Theta, deg

Fig.2b

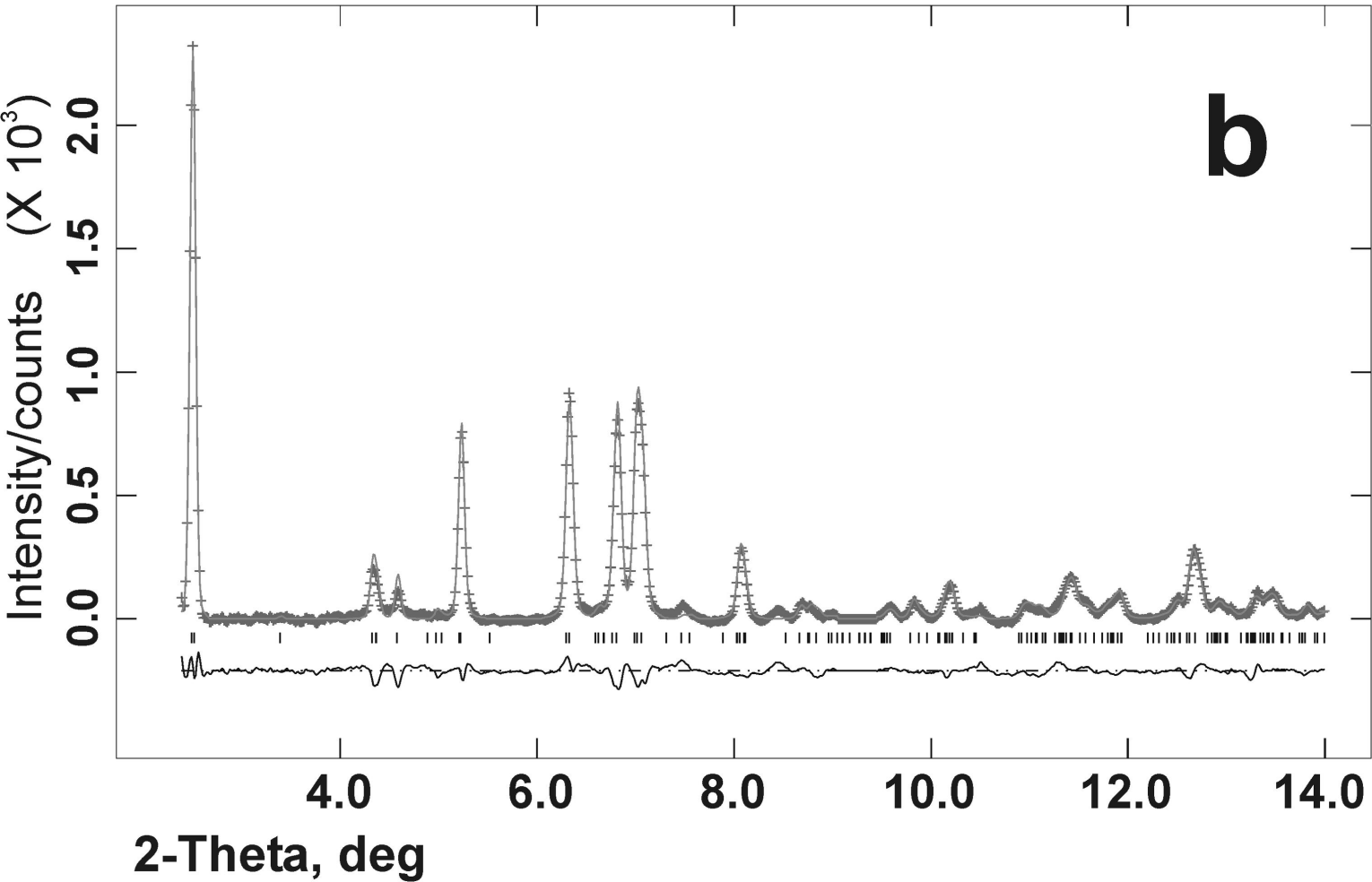
b
Intensity/counts (X 10^3)
0.0
0.5
1.0
1.5
2.0
4.0
6.0
8.0
10.0
12.0
14.0
2-Theta, deg

Fig. 3a

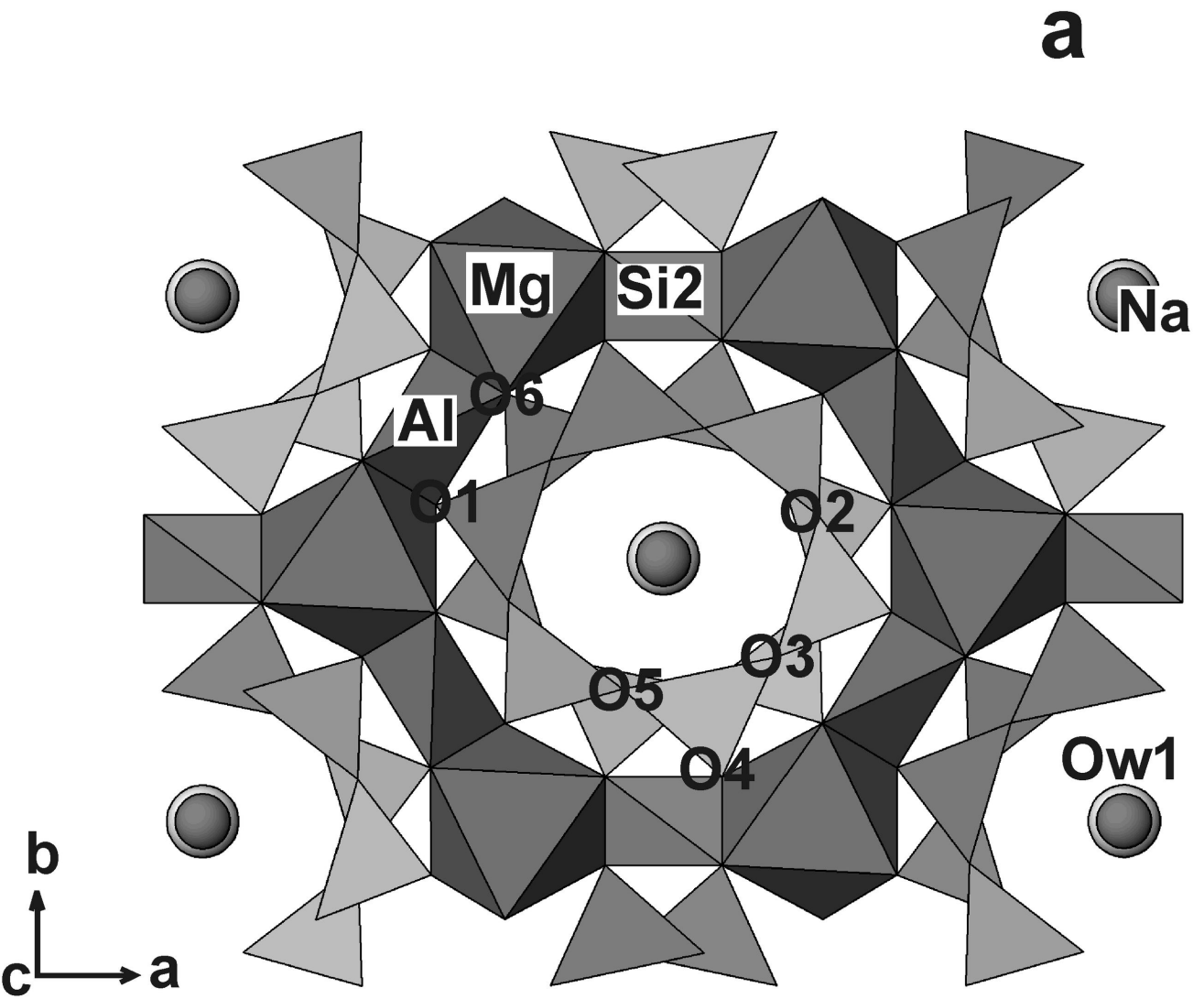

Fig. 3b

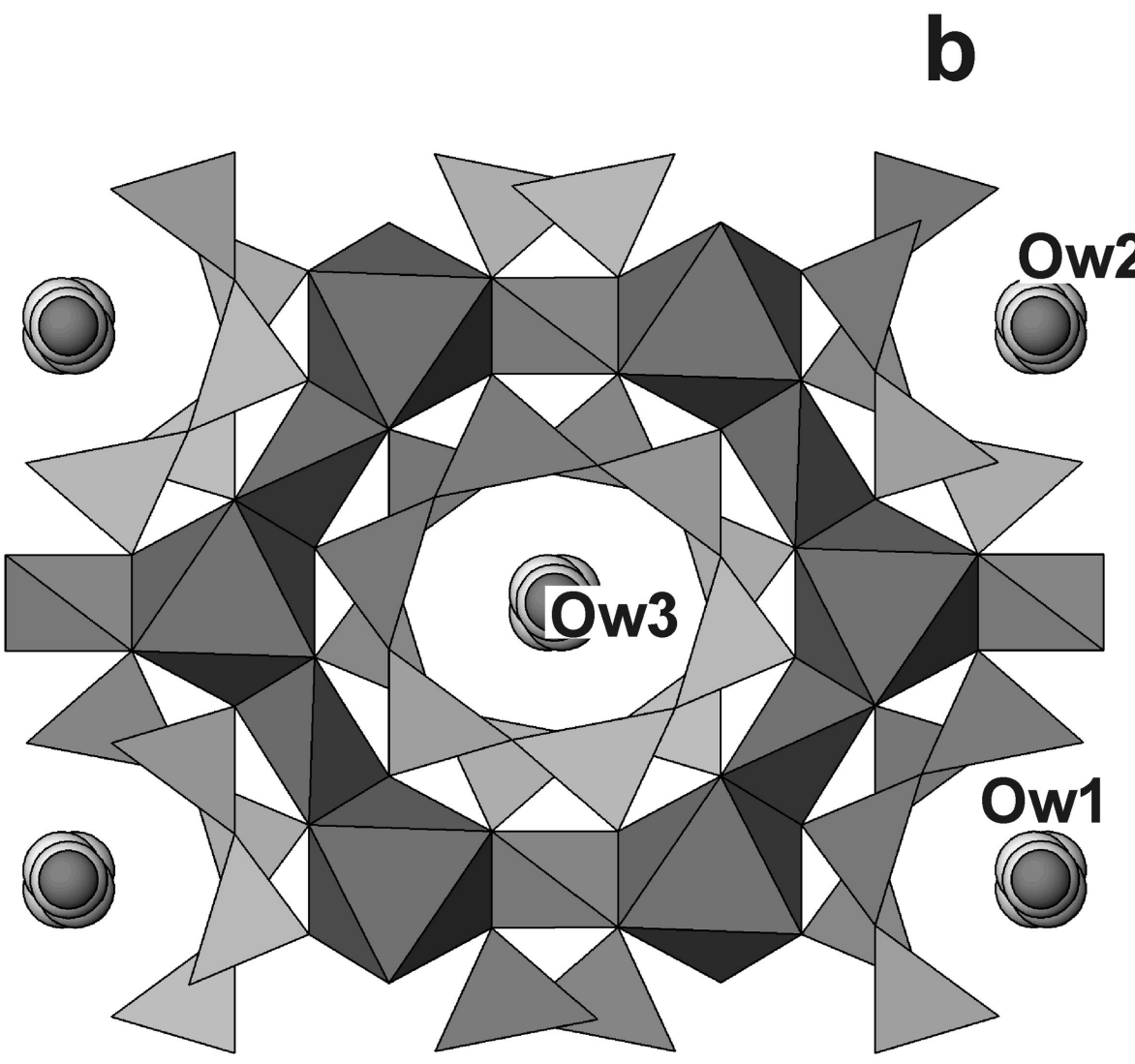

Fig. 3c